Flow biosensing and sampling in indirect electrochemical detection

Francesco Lamberti,[1,a),b)] Camilla Luni,[1,a),b)] Alessandro Zambon,[1,b)] Pier Andrea Serra,[2] Monica Giomo,[1] and Nicola Elvassore[1,b),c)]
[1]*Department of Industrial Engineering, University of Padova, Via Marzolo 9, 35131 Padova, Italy*
[2]*Department of Neuroscience, Medical School, University of Sassari, V.le S. Pietro 43/b, 07100 Sassari, Italy*

(Received 28 February 2012; accepted 5 April 2012; published online 20 April 2012)

Miniaturization in biological analyses has several advantages, such as sample volume reduction and fast response time. The integration of miniaturized biosensors within lab-on-a-chip setups under flow conditions is highly desirable, not only because it simplifies process handling but also because measurements become more robust and operator-independent. In this work, we study the integration of flow amperometric biosensors within a microfluidic platform when analyte concentration is indirectly measured. As a case study, we used a platinum miniaturized glucose biosensor, where glucose is enzymatically converted to H_2O_2 that is oxidized at the electrode. The experimental results produced are strongly coupled to a theoretical analysis of fluid dynamic conditions affecting the electrochemical response of the sensor. We verified that the choice of the inlet flow rate is a critical parameter in flow biosensors, because it affects both glucose and H_2O_2 transport, to and from the electrode. We identify optimal flow rate conditions for accurate sensing at high time resolution. A dimensionless theoretical analysis allows the extension of the results to other sensing systems according to fluid dynamic similarity principles. Furthermore, we developed a microfluidic design that connects a sampling unit to the biosensor, in order to decouple the sampling flow rate from that of the actual measurement. [http://dx.doi.org/10.1063/1.4705368]

I. INTRODUCTION

Miniaturization in biological analyses has several advantages, the most relevant being sample volume reduction, low cost, and relatively fast response time.[1] Furthermore, down-scaling the average dimension of the biosensing device permits to enhance measurement sensitivity exploiting different physical scaling laws.[2] Integrating the analysis step in lab-on-a-chip applications for in-flow process monitoring is highly desirable, not only because it simplifies the handling of the process but also because measurements become more robust and operator-independent.

Online measurements can be advantageously coupled with both *in vitro* experiments and *ex vivo*. Glucose sensors have been implanted in living tissues, but their use is still limited because of the deterioration of sensor performance and inflammatory response.[3] Therefore, non-invasive glucose monitoring seems the most viable alternative in this field and recent commercial products have been produced for performing both extraction and sensing functions,[4] or for coupling with microdialysis.[5,6] Also chemiluminescence metabolite sensors have been integrated into microfluidic platforms,[7] as well as systems based on optical absorbance measurement.[8]

In this frame, electrochemical biosensors represent an interesting approach offering the possibility to combine the analytical capability of electrochemical techniques with the specificity

---

[a)]F. Lamberti and C. Luni contributed equally to this work.
[b)]Also at VIMM—Venetian Institute of Molecular Medicine, Via Orus 2, 35129 Padova, Italy.
[c)]Electronic mail: nicola.elvassore@unipd.it.

of biological recognition processes. The selectivity of these devices can be designed immobilizing a specific biologically active compound such as a cell receptor, an antibody or an enzyme, at the surface of an electrode where it converts the effects of the biological process into a quantitative electric response.[9,10]

For online monitoring miniaturized amperometric biosensors are increasingly used.[11,12] Evaluating their performance when used under flow-through conditions requires an analysis of the effect of working conditions such as flow rate, minimum sample volume, sensitivity, limit of detection, and time resolution of the measurement. In fact, in non-flow conditions, once the biosensing device has been set up, the measurement output is completely defined by the intrinsic physical properties of the species involved, such as enzyme kinetics and diffusion coefficients. On the contrary, in flow-through biosensors, fluid dynamic conditions, depending on the inlet flow rate, affect the measurement output. Different regimes can occur due to the relative characteristic times of the physical phenomena overlapping. A comprehensive study on this topic was pursued by Squires *et al*. for flow-through biosensors that measure the analyte directly.[13,14] However, several biologically interesting compounds, such as glucose, lactate, acetylcholine, and glutamate, are measured by amperometric biosensors with higher accuracy indirectly.[15] In this case, the analyte is converted by specific enzymes into electrochemically detectable components that act as mediators for the measurement.[16] Throughout this work, indirect detection refers to the condition where the actual compound producing the electric signal during the measurement of the analyte is the mediator.

The influence of the flow in indirect measurements has been addressed both in sensor and biosensor electrodes.[17–21] Interestingly, few papers report that increasing the flow rate in indirect enzymatic biosensors the amperometric current decreases.[18,21,22] However, a clear phenomenological explanation have not been properly addressed yet. In this perspective, a rational understanding and the availability of tools that allow to select and realize optimal flow conditions for accurate sensing at high time resolution is of paramount importance for a flexible and cost effective approach in improving the performance of these devices.

In this work, we investigate how the electrochemical measurement of an analyte involving the detection of a mediator is affected by flow conditions in a miniaturized biosensor. As for the experimental results, we focus on a glucose biosensor where glucose is amperometrically detected after its enzymatic conversion to H_2O_2 by glucose oxidase (GOx), according to the following reactions:

$$glucose + O_2 \xrightarrow{GOx} gluconic\ acid + H_2O_2, \tag{1}$$

$$H_2O_2 \xrightarrow{electrode} O_2 + 2H^+ + 2e^-. \tag{2}$$

In this system, the current variation is affected by glucose and peroxide mass transport within the microfluidic channel. The experimental setup serves as a case study within a more general investigation of the behavior of indirect analyte detection. A model-based theoretical analysis allows a generalization of the results and represents a tool for design and optimization of flow-through biosensing devices. Moreover, biosensor performance can be improved by decoupling sampling and analysis systems whenever a different flow rate is required for optimal sampling and analysis process. Although there are few papers discussing indirect flow biosensing using a decoupled experimental configuration,[23–26] we propose an improved design of a flow sampling and biosensing unit easy to incorporate in lab-on-a-chip applications.

II. METHODS

A. Device description

The biosensor used in this work was produced modifying a previously described procedure[27] and is shown in Fig. 1. As highlighted in the schematic view in Fig. 1(a), the fluid sample enters in the system and passes the reference (R), counter (C), and working (W) electrodes.

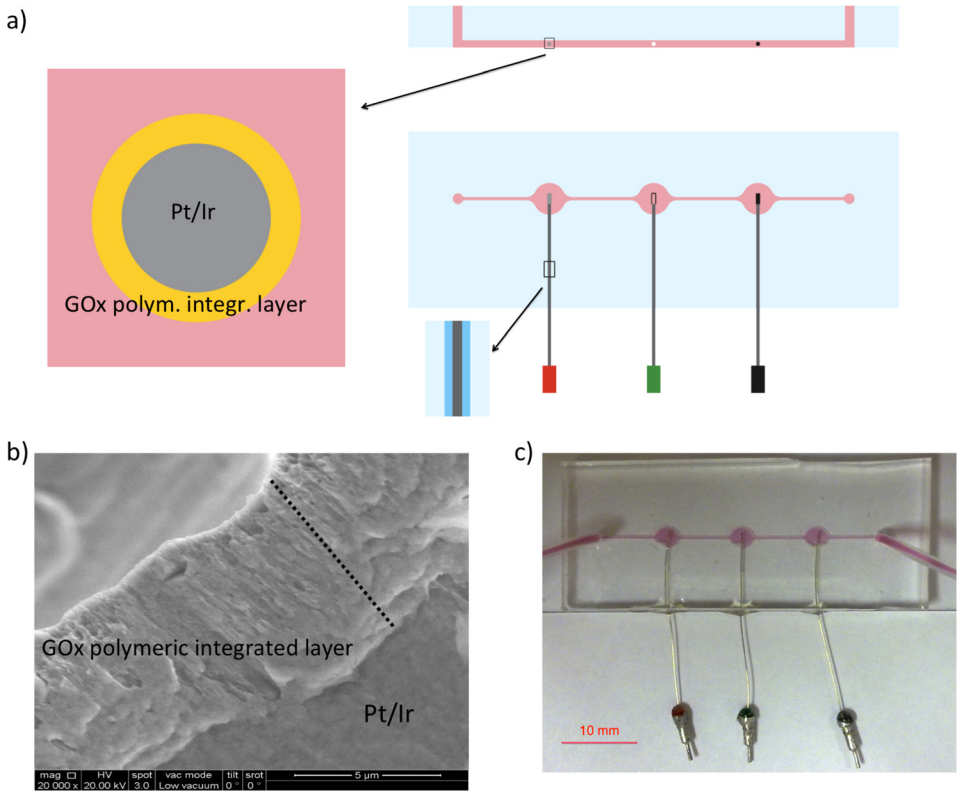

FIG. 1. Microfluidic biosensor. (a) Lateral and top views of the main channel. Working (red), reference (green), and counter (black) electrodes. Enlargements of the transversal and longitudinal sections of the working electrode tip and of the insulated part, not on scale. (b) Scanning electron micrograph of the transversal section of the electrode tip: a GOx polyurethane integrated layer, whose thickness is indicated by the dotted line, coats a Pt/Ir wire. (c) Picture of the microfluidic system schematically described in (a) with pink medium flowing.

The distance between reference and working electrodes is sufficiently small not to affect the measurement, as we tested interchanging electrode positions. The enlargement of the channel section at the electrodes guarantees complete wetting of the sensing tip in case of bubble formation at the walls. The 1-mm long electrode tip, made of Pt/Ir 90/10% and with a diameter of 125 μm, is coated with a porous polymeric layer (polyethylenimine and polyurethane) absorbed with the enzyme glucose oxidase (GOx) from Aspergillus Niger. This GOx-integrated layer was estimated by scanning electron microscopy to be approximately 8 μm thick (Fig. 1(b)). The stability of GOx in this structure was extensively studied by our group[28,29] and others.[30] Glucose is enzymatically converted into H_2O_2 in the porous layer, and the electrochemical oxidation of H_2O_2 at the electrode produces the amperometric current measured. The polymeric layer did not show observable damage due to the production of oxygen and H_2O_2 for the whole duration of the experiments. The biosensor was calibrated under static conditions (Fig. S1 of the supplementary material[31]) and then used for flow-through measurements.

B. Microfabrication

1. Microfluidic sensing

A single-layer channel (300 μm), containing the biosensors lateral inlets (400 μm), was made using soft lithographic techniques[32,33] (Fig. 1(a)). The silicon substrate was coated with SU8-2100 (MicroChem Corp., MA,USA) to obtain a thickness of 250 μm. Then, soft bake, exposure, and post-exposure bake followed the coating. The development was achieved in methoxymetacrilate (Sigma-Aldrich, Italy) and further rising with Isopropanol. Polydimethylsiloxane (PDMS,

Dow Corning, USA) was used for molding in the ratio 10:1 (base:cure agent) and baked at 353 K for 2 hours.

The cured PDMS chip was bounded to a borosilicate glass (Vetrotecnica Italy) by plasma treatment (70 W, 30 s). After the wires insertion, the lateral inlets were sealed using UV glue (DYMAX Corp., USA) that was polymerized *in situ* using a UV lamp for 5 s (DYMAX 3067, USA). A syringe pump (PHD 22/2000 HPSI, Harvard Apparatus, USA) connected to the chip via 0.02 in. inner diameter Tygon tubing, allowed to change the flow rate. Syringes of 3 - and 5-ml volume (Becton Dickinson, USA) were used to obtain the desired fluid flow.

2. Microfluidic sampling and sensing

To create the loop system, containing flow and control channels,[34,35] two molds were prepared. 36 μm of SPR 220-7 (Dow Corning) were spun on a vapor-treated silicon wafer HDMS (Sigma Aldrich). After bake at 363 K for 90 min and rehydration for 3 h, each mold was exposed at 200 mJ/cm^2 ($\lambda = 365$ nm, OAI 150, USA). 400 μm-wide flow layer channels were obtained by development in agitated MF319 (Dow Corning) and further rinsing with D-water. A hard baking up to 463 K with 10 K/h ramp was done to reflow the polymer and obtain round channels. For the control layer, SU8-2100 (Microchem Corporation) was used to make square channels of 100 μm height and 300 μm width. PDMS (10:1 base:cure agent) was spun on the flow mold at 1000 rpm for 90 s to obtain a thin membrane of 80 μm in total. The control mold was covered instead with a thick layer of PDMS and both layers were then baked at 353 K for 30 min. A further very thin layer of cure agent was painted on the flow mold, and the control chip was then aligned on it. A further baking for 2 h produces irreversible bonding between the two layers. The final chip was bonded via plasma treatment to a borosilicate glass. The valves were activated pressurizing the control channels.

C. Potentiostatic measurements

Potentiostatic amperometric measurements were performed using a potentiostat/galvanostat (AUTOLAB, PGSTAT 128 N EcoChemie, The Netherlands) controlled by NOVA 1.6 Software. The biosensor was used as the working electrode, a Pt wire as the counter electrode and Ag/AgCl as the pseudo-reference (Fig. 1(a)). The working electrode was biased 0.7 V versus the pseudo-reference electrode. Static measurements were performed for calibration in usual electrochemical commercial cells, outside the microfluidic chip. Static calibration was used as a performance check on the sensor before integration in the microfluidic channel. Solutions used were PBS 1X (Vetrotecnica, Italy), 1 mM Dulbecco's Modified Eagle Medium High Glucose (DMEM High Glucose, 4.5 mg/l D-Glucose, Invitrogen, Italy), 5 mM Dulbecco's Modified Eagle Medium Glucose free (DMEM Glucose Free, Invitrogen, Italy), and H_2O_2 solutions prepared by diluting 80% H_2O_2 (Sigma-Aldrich, Italy) with milliQ water (Millipore, Italy). All solution used were sterile.

D. Mathematical model

1. Numerical mathematical model

A mathematical model of the steady-state flow biosensing device was developed. The system geometry includes: a microfluidic channel, a cylindrical electrode inserted across the channel, and a porous layer coating the electrode and containing GOx. The 2-dimensional model represents a longitudinal section of the device described. Modeling was carried out breaking the system down into two sub-domains: the microfluidic channel and the porous layer coating the electrode. As for the microfluidic channel, both convective and diffusive transport are described. While in the porous layer coating the electrode, glucose conversion by a homogeneously distributed enzyme is modeled together with diffusion. The velocity field in the microfluidic channel was obtained solving the continuity equation and the equation of motion for an incompressible Newtonian fluid. The concentration fields of H_2O_2 and glucose were obtained in the microfluidic channel and in the porous layer, solving the respective equations of continuity. The effective diffusivities in the

porous layer were obtained multiplying their bulk values, $D_{glucose,bulk}$ and $D_{H_2O_2,bulk}$, by a factor, ϵ, accounting for both the porosity and tortuosity of the material. The rate of glucose conversion, catalyzed by GOx in the porous layer, was assumed linear with kinetic parameter k_{GOx}, a good approximation in the glucose concentration range simulated.

The electric current, I, produced at the electrode, is given by

$$I = 2 \cdot F \cdot \int_{S_{el}} F_{H_2O_2,el} dS_{el}, \tag{3}$$

where the factor 2 represents the number of electrons involved in the charge transfer at the electrode surface according to Eq. (2), F is Faraday's constant, $F_{H_2O_2,el}$ is H_2O_2 molar flux at the electrode, and S_{el} is the geometrical electrode surface. In the simulations where a flow containing only H_2O_2 enters the system, the actual current value was obtained multiplying I by a corrective factor, λ. This correction accounts for the observed reduction of current in these conditions, probably due to a net production of O_2 polarizing the electrode. The model was numerically solved by COMSOL MULTIPHYSICS (COMSOL, Inc, Stockholm, Sweden) using the parameter values summarized in Table I. In particular, model parameters ϵ, k_{GOx}, and λ were determined by fitting the experimental data. Details on the numerical model are reported in the supplementary material.[31]

2. Analytical mathematical model

The model equations for glucose and H_2O_2 in the porous layer coating the electrode were also solved analytically under steady-state conditions for a simplified geometry, i.e., a flat electrode with the same surface area of the electrode considered in the numerical model. Details of analytical model development are reported in the supplementary material.[31] The fluxes of glucose and H_2O_2 across the surface of the porous layer, $F_{glucose,b/l}$ and $F_{H_2O_2,b/l}$, are related to the Reynolds number, Re, at the entrance of the convective system by

$$F_{glucose,b/l} = \frac{D_{glucose,bulk} \cdot \left(c_{glucose,in} - c_{glucose,b/l}\right)}{H} \cdot \alpha \cdot Re^{\beta}, \tag{4}$$

and

$$F_{H_2O_2,b/l} = \frac{D_{H_2O_2,bulk} \cdot \left(c_{H_2O_2,in} - c_{H_2O_2,b/l}\right)}{H} \cdot \alpha \cdot Re^{\beta}, \tag{5}$$

TABLE I. Values of the parameter used in the solution of the mathematical model.

Parameter	Value	Ref.
L (m)	$0.705 \cdot 10^{-3}$	—
H (m)	$0.282 \cdot 10^{-3}$	—
W (m)	$2 \cdot 10^{-3}$	—
D_i (m)	$0.125 \cdot 10^{-3}$	—
L_{tip} (m)	$1 \cdot 10^{-3}$	—
δ (m)	$8 \cdot 10^{-6}$	—
μ (Pa · s)	$7.16 \cdot 10^{-4}$	36
ρ (kg/m^3)	993.45	36
$D_{glucose,bulk}$ (m^2/s)	$6 \cdot 10^{-10}$	37
$D_{H_2O_2,bulk}$ (m^2/s)	$1.83 \cdot 10^{-9}$	38
ϵ	0.145	Estimated
k_{GOx} (1/s)	0.015	Estimated
λ	0.02	Estimated

where $c_{glucose,in}$ and $c_{H_2O_2,in}$ are glucose and H_2O_2 concentrations at the entrance of the convective system, $c_{glucose,b/l}$ and $c_{H_2O_2,b/l}$ at the surface of the porous layer, H is the convective system characteristic length (the channel height in the numerical model), α and β are constants, whose values are determined according to fluid dynamic similarity principles, as explained in the supplementary material.[31]

III. RESULTS AND DISCUSSION

A. Effect of fluid flow

Extending the use of an electrochemical biosensor with indirect detection to flow working conditions, requires the definition of an optimal flow rate. We analyzed the mass transport mechanisms occurring, both experimentally and theoretically.

In order to evaluate how fluid dynamic affects the biosensor behavior, a set of experiments was carried out feeding a solution containing H_2O_2. In this way, it is possible to highlight the effect of the flow rate on the direct electrochemical measurement of the solute, without the overlapping kinetics of the intermediate production. Results highlight that at low flow rates the overall process is limited by mass transport through the stagnant layer in the liquid domain surrounding

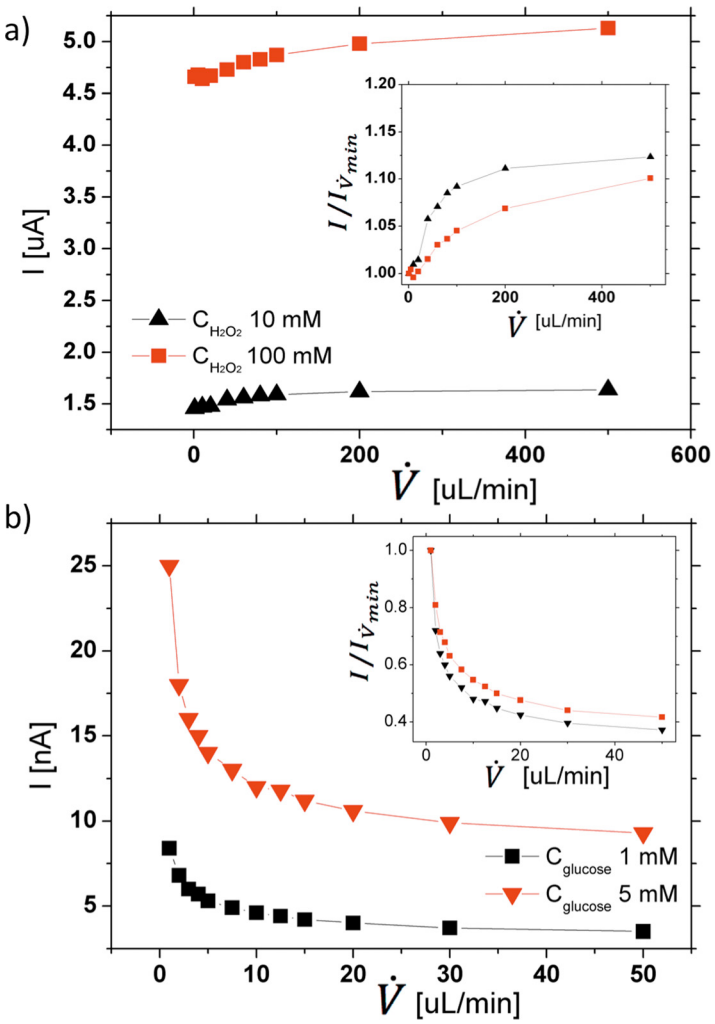

FIG. 2. Effect of flow rate on (a) hydrogen peroxide and (b) glucose in-flow detection at different concentrations. The current collected at the electrode is plotted as a function of the flow rate. Inset graphs show the current normalized by its value at the minimum flow rate used in the experiments (1 μl/min), $I_{\dot{V}_{min}}$.

the porous coating. The current increases at increasing flow rates because this diffusive stagnant layer gets thinner (Fig. 2(a)). Then, current tends to a plateau at very high flow rates, when the external mass transport becomes faster and the overall mass transport is only limited by diffusion of species in the porous coating. However, the current variation detected is only approximately 10%, even for large differences in the flow rate, from 10 μl/min to 400 μl/min (Fig. 2(a), inset). This behavior is barely affected by concentration, as verified with a change of one order of magnitude, from 10 to 100 mM (Fig. 2(a), inset).

Then, we studied the effect of the flow rate for biologically relevant working conditions of the biosensor, i.e., with a glucose solution in the concentration range 1–5 mM, entering the system with flow rates of 1–50 μl/min. In this case, the current detected decreases at increasing flow rates (Fig. 2(b)), for both glucose concentrations used (1 and 5 mM) confirming literature data.[39] In particular, it decreases of about 60% in the flow rate range tested, while the concentration negligibly affects this behavior (Fig. 2(b), inset).

These observations show how using an electrochemical biosensor with enzyme-mediated detection under flow conditions requires a careful understanding of the phenomena that come into play, posing the flow rate as a key variable to analyze. These experimental observations for glucose amperometric detection are fully consistent with those reported in literature,[18,21,22] whereas H_2O_2 analyses allow the dissection of the contribution of flow rate influence on substrate and mediator detection.

B. Efficiency and time of response of the biosensor

For practical purposes, the effective efficiency, η_{eff}, for an indirect electrochemical biosensor, can be defined by the following expression:

$$\eta_{eff} = \frac{I_{glucose}}{I_{H_2O_2}}, \tag{6}$$

where $I_{glucose}$ and $I_{H_2O_2}$ stand for the current produced when a glucose or a stoichiometric H_2O_2 solution enters the system, respectively. $I_{H_2O_2}$ represents the maximum amount of H_2O_2 detectable at the electrode if all glucose flowing through the system were converted. Fig. 3(a) shows how the efficiency, calculated according to Eq. (6), decreases as a function of the flow rate.

Furthermore, flow rate also affects the biosensor time of response, which is the time needed to detect a stable current for constant inlet conditions (Fig. S3 of the supplementary material[31]). The time of response is an important variable for biosensor use because it determines the maximum temporal resolution, i.e., the smallest increment of time between two successive measurements. Fig. 3(b) shows that the time of response is a decreasing function of the flow rate. Thus, in order to have a high-performance online, biosensor an optimal flow rate is required as a trade-off between high efficiency and high time resolution.

C. Numerical simulations

Experimental data suggest a flow rate-dependent leak of H_2O_2, not oxidizing at the electrode and decreasing the measurement efficiency. We further investigated the physical phenomena occurring within the biosensor by means of a mathematical model. The geometry of the system simulated closely reproduces the experimental setup and is described in Fig. 4(a). Convective flow occurs in bulk medium along the x-direction, while a cylindrical electrode tip is placed across the flow along the z-direction. Glucose is converted into H_2O_2 in the porous layer coating the electrode. Both species move within this layer exclusively by diffusion according to a concentration gradient. Part of the H_2O_2 produced reaches the electrode where it is immediately oxidized, while part of it leaves the porous layer at the external surface and is washed out by the convective flow.

Figs. 4(b) and 4(c) illustrate H_2O_2 concentration profiles obtained by the model at two flow rates, 1 and 50 μl/min, respectively. At low flow rates, a concentration gradient develops

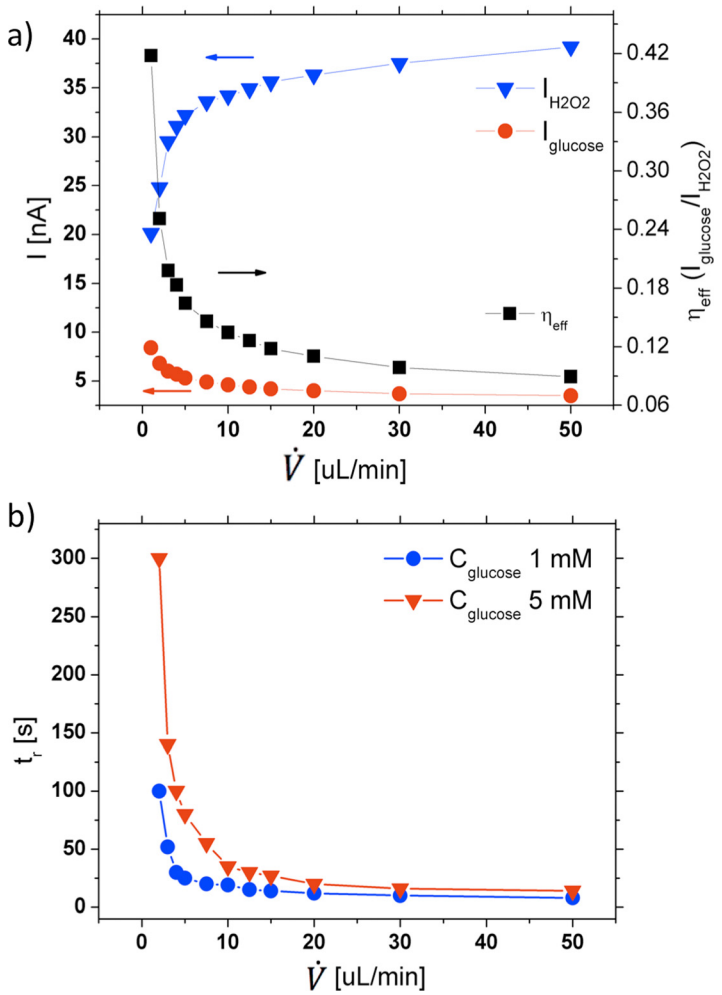

FIG. 3. Effect of flow rate on measurement efficiency and response time of the biosensor. (a) The currents $I_{glucose}$ and $I_{H_2O_2}$ detected when measuring samples with concentrations of 1 mM glucose and 1 mM H_2O_2, respectively, are plotted as a function of the flow rate. They are used to calculate the efficiency, η_{eff}, defined as the ratio of $I_{glucose}$ to $I_{H_2O_2}$, also shown. (b) Biosensor response time (Fig. S3 of supplementary material[31]) as a function of flow rate for two different inlet concentrations.

throughout the channel section (Fig. 4(b)), while at high flow rates, H_2O_2 is rapidly washed-out and its bulk concentration is about null at short distance outside the porous layer (Fig. 4(c)).

The results from the numerical model simulations confirm the experimental data presented in Fig. 3(a), and, specifically, show a decreasing efficiency at higher flow rates (Fig. 4(f)). We further investigate this aspect in Fig. 4(g), after calculating two non-dimensional quantities: $Ratio_{glucose}$ and $Ratio_{H_2O_2}$. $Ratio_{glucose}$ is defined as the ratio of the total glucose consumed per unit time to the glucose molar flow rate entering the system, according to the following expression:

$$Ratio_{glucose} = \frac{N_{glucose,rx}}{N_{glucose,in}} \tag{7}$$

and $Ratio_{H_2O_2}$ are given by the ratio of the H_2O_2 molar flow rate leaving the porous layer towards the bulk to the total H_2O_2 produced per unit time in the layer, that is

$$Ratio_{H_2O_2} = \frac{N_{H_2O_2,out}}{N_{H_2O_2,rx}}. \tag{8}$$

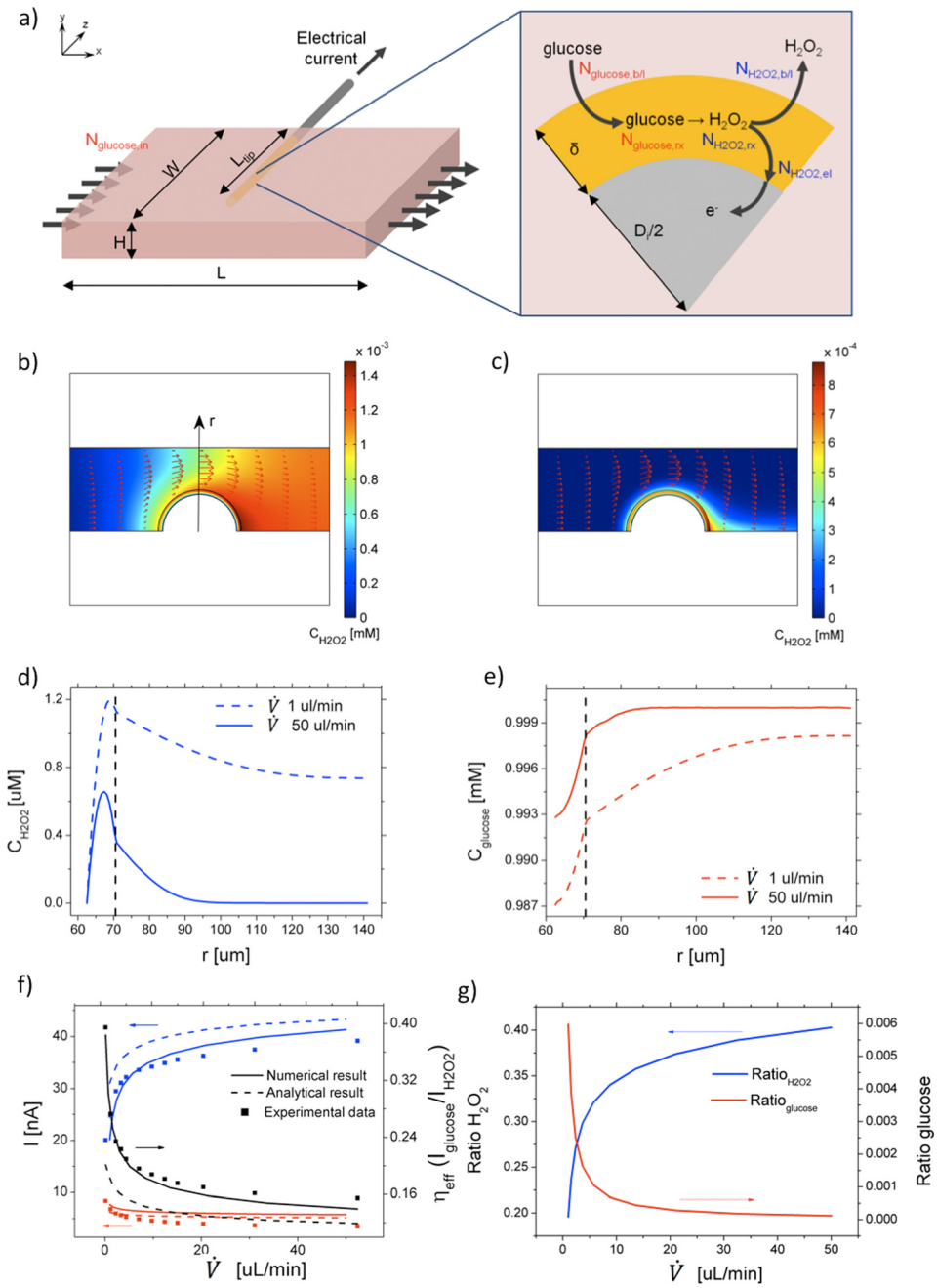

FIG. 4. Results obtained from the simulations of the numerical model. (a) Schematic representation of the model geometry. System size, coordinate system, and molar flow rates of glucose and H_2O_2 are also indicated. (b) and (c) Concentration profile of H_2O_2 in the channel and in the porous layer coating the electrode surface when a 1-mM solution of glucose is fed to the system at two flow rates: 1 μl/min (b) and 50 μl/min (c). Red arrows represent the velocity field. (d) and (e) Concentration profiles of H_2O_2 and glucose along the r-axis indicated in (b), obtained under the same conditions of (b) and (c). The black dashed line indicates the edge of the porous layer coating the electrode. (f) Comparison of the electric current discharged at the electrode as a function of the flow rate obtained experimentally and by the numerical and analytical models. Red lines refer to an inlet of 1-mM glucose solution, blue lines to a 1-mM H_2O_2 solution. Efficiency, η_{eff}, given by the ratio of the two currents, is displayed in black. The comparison is qualitative because geometries are not identical in the three cases, as discussed in the main text. (g) $Ratio_{H_2O_2}$ and $Ratio_{glucose}$, defined in Eqs. (7) and (8), are shown as a function of the flow rate.

The flow rates in Eqs. (7) and (8) are defined in Fig. 4(a). $Ratio_{glucose}$ decreases at increasing volumetric flow rates, because a larger amount of glucose flows through the system without having time to diffuse in the porous layer (Fig. 4(g)). On the contrary, $Ratio_{H_2O_2}$ increases at higher flow rates (Fig. 4(g)), that is, a larger amount of H_2O_2 is washed-out from the porous layer without oxidizing at the electrode, what explains the decrease of measurement efficiency.

The numerical model is also able to give H_2O_2 and glucose concentration profiles in the channel along the r-coordinate highlighted in Fig. 4(b). H_2O_2 concentration shows a peak inside the porous layer coating the electrode (Fig. 4(d)), whose position depends on the relative importance of the two molar flow rates, $N_{H_2O_2,b/l}$ and $N_{H_2O_2,el}$, defined in Fig. 4(a). On the contrary, glucose concentration along the same direction shows a monotonic profile, as all glucose entering the layer is converted to H_2O_2 (Fig. 4(e)). The GOx-catalyzed reaction occurs throughout the whole thickness of the porous layer in our system, as demonstrated by the only slight decrease of glucose concentration in the layer (Fig. 4(e)). This is confirmed by the high rate of glucose diffusion in the layer compared to the reaction rate, about ten times larger.

Taken together both experimental and computational observations show that glucose efficiency reduction at higher flow rates is related to the ratio between H_2O_2 wash-out and discharge at the electrode. In order to extend this result to a wider class of biosensors, we derived a simple analytical model as a function of dimensionless variables taking into account all the transport phenomena involved.

D. Analytical results

We analytically solved the mathematical model in the porous layer for the simplified geometry previously described, to obtain a rational insight into the experimental data. The resulting efficiency, η, given by the ratio of the current produced feeding a glucose solution to that produced feeding a stoichiometric H_2O_2 solution, is analytically expressed as

$$\eta = \frac{D_{glucose,bulk}}{D_{H_2O_2,bulk}} \cdot \left[1 - \frac{1}{\cosh\phi + \frac{R_g \cdot \phi}{\alpha \cdot Re^{\beta}} \cdot \sinh\phi} \right], \tag{9}$$

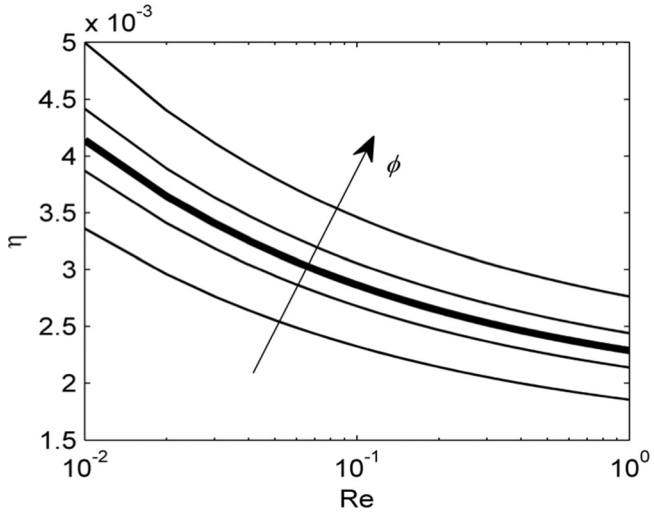

FIG. 5. Dimensionless results of biosensor efficiency, η. Efficiency is plotted as a function of Reynolds number, according to Eq. (9), within the range used in the experiments. Curves are parametric in Thiele's modulus, in the range ±10% of the experimental Thiele's modulus, shown by the thicker line.

where $R_g = \epsilon \cdot H/\delta$ is a dimensionless geometric ratio, $\phi = \delta\sqrt{k_{GOx}/\left(\epsilon \cdot D_{glucose,bulk}\right)}$ is Thiele's modulus. All other variables are defined in Fig. 4(a) and Sec. II. η is a theoretical efficiency and neglects the reduction of current occurring when feeding an H_2O_2 solution. Thus, it is related to η_{eff} by the following expression: $\eta = \eta_{eff} \cdot \lambda$. Expression (9) shows that, once defined geometry and physical properties of the system, the efficiency only depends on Reynolds number, Re, which is proportional to the volumetric flow rate. For Re$\rightarrow$ 0, the efficiency η tends to its maximum, equal to the ratio of the bulk diffusivities, $D_{glucose,bulk}/D_{H_2O_2,bulk}$, always less than one because of the relative size of the two species.

Keeping constant the diffusivity and the geometric ratios, we studied the dependence of the efficiency from Re and Thiele's modulus (Fig. 5). η is a decreasing function of Re, and this further confirms the experimental trend. A comparison between experimental, numerical, and analytical results is presented in Fig. 4(f). The slight discrepancies are due to the increasingly simplified geometry between the three systems. However, the shape of the profiles is confirmed in all cases. Thiele's modulus quantifies the ratio of the reaction rate to the diffusion rate in the porous layer. When glucose conversion to H_2O_2 is fast in comparison with the mass transfer rate in the layer (high ϕ), efficiency increases, because glucose concentration gradient through the layer is larger in these conditions, and consequently the diffusive flow of glucose into the layer is greater.

It is worth to highlight that Eq. (9) can be easily extended to different enzymatic biosensors by changing the intrinsic properties of the substances involved. Although it is an approximated solution of a more complex system, it can be used to properly analyse the effect of fluid dynamics on substrate detection assisting the identification of optimal operative conditions.

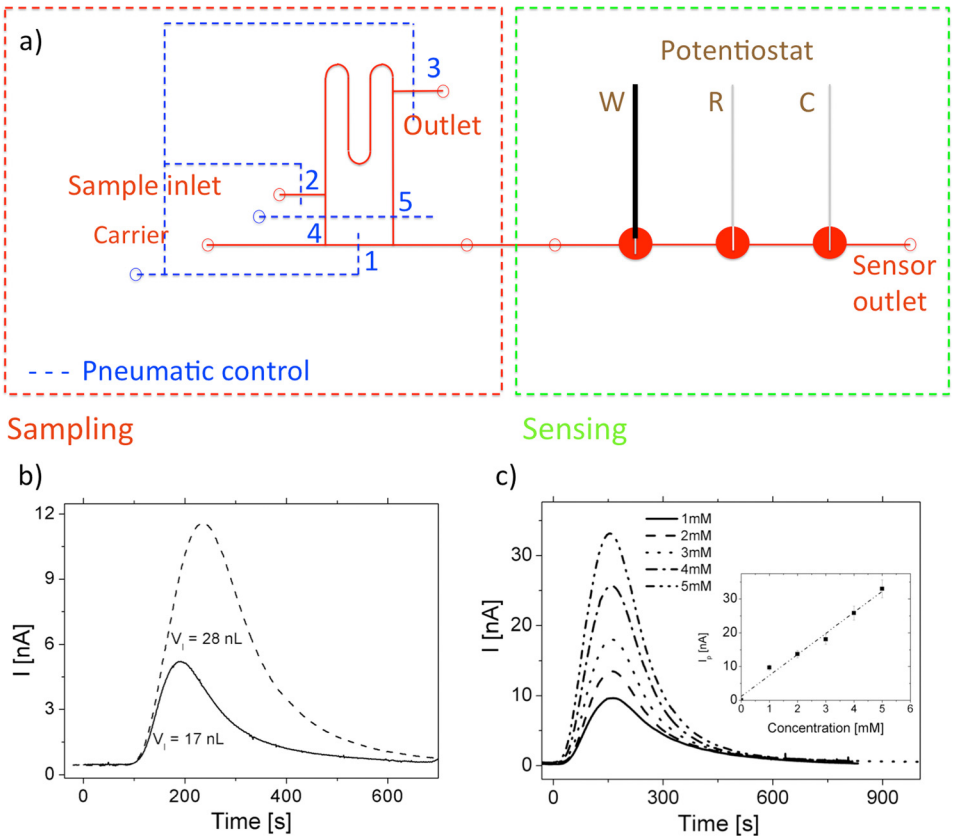

FIG. 6. Sampling and sensing units integration. (a) Schematic view of the entire system. Loop loading: open 1, 2, 3; close 4, 5. Sample analysis: open 1, 2, 3; close 4, 5. (b) Amperometric measurement for two loop volumes, V_l. Sample glucose concentration is 2 mM and flow rate is 10 μl/min. (c) Amperometric measurement for a 28-nl loop at different glucose concentrations in the range 1-5 mM. Flow rate is 10 μl/min. The inset shows the dependence of the peak current, I_p, from glucose concentration. Squares represent experimental data (error bars indicate standard deviations), and the dashed line the linear fitting regression.

E. Decoupling system

The previous analysis highlighted the importance to control the volumetric flow rate during biosensor use. For this reason, we developed a new design for performing biosensing measurements that decouples the flow rate used for the measurement from the sampling flow rate. The new system includes a loop filled offline with the sample at an independent flow rate respect to that in the main channel (Fig. 6(a)). The loop is connected to the main inlet through a valve system and can be connected/disconnected (on/off) when requested (Fig. S4 of the supplementary material[31]). The advantage of this design is to fill the loop at high flow rates, when it is switched off during sampling, and to have the sample entering near the working electrode at a low independent flow rate when it is switched on. As an example, in this work, a sensing flow rate of 10 μl/min was used to obtain a response time of less than 1 min (Fig. 3).

Instead of having a plateau in the current detected, a peak shape response is obtained because of the finite volume of the loop (Figs. 6(b) and 6(c)). Larger loops produce higher peaks of current, as shown in Fig. 6(b) for two different loop volumes (17 and 28 nl). Depending on the sample amount available and the temporal resolution required, the loop volume should be chosen to increase biosensor sensitivity, which is 6.22 nA/mM for the 28-nl loop.

The peak maximum of the current curve is taken as the measurement value of glucose concentration. We verified that this measure is proportional to glucose concentration in the sample for a fixed loop volume and thus represents a reliable measurement (Fig. 6(c)). The response time at these conditions is about 100 s (Fig. 6(c)). The biosensor works under highly controlled conditions, measurements are very repeatable, and the linearity of the response is independent from the loop volume (Fig. S5 of the supplementary material[31]). The detection limit is 0.18 mM for the 28-nl loop, which is very low compared to other electrochemical biosensors in the literature.[40] Instead, electrochemical sensors for H_2O_2 detection, have a lower limit, in the range 2–15 μM.[41,42]

IV. CONCLUSIONS

We have studied the effect of convective flow in the indirect amperometric detection of an analyte. The experimental results were obtained for the case study of a glucose miniaturized biosensor. The proposed model-based theoretical analysis gives generality to these results. The outcome shows that the fluid flow rate plays a significant role in the performance of the biosensor. In particular, for high-time resolution and high-efficiency measurements, the choice of flow rate requires optimization. The good quantitative agreement between experimental data and numerical predictions shows that the mathematical model can be advantageously used to define the more suitable operating conditions for online indirect detection. All together these results show that with flow conditions the mediator wash-out can be a critical point in all electrochemical indirect measurements. We also developed a lab-on-a-chip application for integrated sampling and biosensing that decouples the two flow rates allowing their independent control. This offers a reliable and robust method of detection that can be easily incorporated in biological experiments for online in-flow measurements.

ACKNOWLEDGMENTS

This research was supported by University of Padova and by the Italian Ministry of Research.

[1]K. Liu, R. Wu, Y. Chuang, H. Khoo, S. Huang, and F. Tseng, "Microfluidic systems for biosensing," Sensors **10**, 6623–6661 (2010).
[2]E. Verpoorte, "Microfluidic chips for clinical and forensic analysis," Electrophoresis **23**, 677–712 (2002).
[3]M. Frost and M. Meyerhoff, "*In vivo* chemical sensors: Tackling biocompatibility," Anal. Chem. **78**, 7370–7377 (2006).
[4]M. Tierney, H. Kim, M. Burns, J. Tamada, and R. Potts, "Electroanalysis of glucose in transcutaneously extracted samples," Electroanalysis **12**, 666–671 (2000).
[5]R. Rhemrev-Boom, R. Tiessen, A. Jonker, K. Venema, P. Vadgama, and J. Korf, "A lightweight measuring device for the continuous *in vivo* monitoring of glucose by means of ultraslow microdialysis in combination with a miniaturised flow-through biosensor," Clin. Chim. Acta **316**, 1–10 (2002).
[6]A. Maran, C. Crepaldi, A. Avogaro, S. Catuogno, A. Burlina, A. Poscia, and A. Tiengo, "Continuous glucose monitoring in conditions other than diabetes," Diabetes/Metab.Res. Rev. **20**, S50–S55 (2004).

[7]Y. Lv, Z. Zhang, and F. Chen, "Chemiluminescence microfluidic system sensor on a chip for determination of glucose in human serum with immobilized reagents," Talanta **59**, 571–576 (2003).
[8]V. Srinivasan, V. Pamula, M. Pollack, and R. Fair, "A digital microfluidic biosensor for multianalyte detection," in *IEEE The Sixteenth Annual International Conference on Micro Electro Mechanical Systems, 2003. MEMS-03 Kyoto* (IEEE, 2003), pp. 327–330.
[9]G. Harwood and C. Pouton, "Amperometric enzyme biosensors for the analysis of drugs and metabolites," Adv. Drug Delivery Rev. **18**, 163–191 (1996).
[10]S. Borgmann, A. Schulte, S. Neugebauer, and W. Schuhmann, "Amperometric biosensors," Adv. Electrochem. Sci. Eng. 1–83 (2012).
[11]J. Wang, "Amperometric biosensors for clinical and therapeutic drug monitoring: A review," J. Pharm. Biomed. Anal. **19**, 47–53 (1999).
[12]E. Zilkha, T. Obrenovitch, A. Koshy, H. Kusakabe, and H. Bennetto, "Extracellular glutamate: On-line monitoring using microdialysis coupled to enzyme-amperometric analysis," J. Neurosci. Methods **60**, 1–9 (1995).
[13]T. Squires and S. Quake, "Microfluidics: Fluid physics at the nanoliter scale," Rev. Mod. **77**, 977 (2005).
[14]T. Squires, R. Messinger, and S. Manalis, "Making it stick: Convection, reaction and diffusion in surface-based biosensors," Nature Biotechnol. **26**, 417–426 (2008).
[15]F. Lamberti, M. Giomo, and N. Elvassore, *Carbon Nanotubes: Growth and Applications*, Electrochemical Biosensing with Carbon Nanotubes, edited by M. Naraghi (Intech, 2011).
[16]P. Pantano and W. Kuhr, "Enzyme-modified microelectrodes for *in vivo* neurochemical measurements," Electroanalysis **7**, 405–416 (1995).
[17]W. Breen, J. Cassidy, and M. Lyons, "Theoretical study of permselective layers on amperometric electrodes in flowing streams," Anal. Chem. **63**, 2263–2268 (1991).
[18]F. Palmisano, D. Centonze, and P. Zambonin, "An *in situ* electrosynthesized amperometric biosensor based on lactate oxidase immobilized in a poly-o-phenylenediamine film: Determination of lactate in serum by flow injection analysis," Biosens. Bioelectron. **9**, 471–479 (1994).
[19]J. Cooper and R. Compton, "Channel electrodesa review," Electroanalysis **10**, 141–155 (1998).
[20]N. P. Rodrigues, Y. Sakai, and T. Fujii, "Cell-based microfluidic biochip for the electrochemical real-time monitoring of glucose and oxygen," Sens. Actuators B **132**, 608–613 (2008).
[21]O. Frey, S. Talaei, P. van der Wal, M. Koudelka-Hep, and N. de Rooij, "Continuous-flow multi-analyte biosensor cartridge with controllable linear response range," Lab Chip **10**, 2226–2234 (2010).
[22]M. Hashimoto, S. Upadhyay, and H. Suzuki, "Dependence of the response of an amperometric biosensor formed in a micro flow channel on structural and conditional parameters," Biosens. Bioelectron. **21**, 2224–2231 (2006).
[23]R. Appelqvist, G. Markovarga, L. Gorton, A. Torstensson, and G. Johansson, "Enzymatic determination of glucose in a flow system by catalytic-oxidation of the nicotinamide coenzime at a modified electrode," Anal. Chim. Acta **169**, 237–247 (1985).
[24]Q. J. Chi and S. J. Dong, "Flow-injection analysis of glucose at an amperometric glucose sensor-based on electrochemical codeposition of pallaium and glucose-oxidase on a glassy-carbon electrode," Anal. Chim. Acta **278**, 17–23 (1993).
[25]F. Mizutani and S. Yabuki, "Flow injection analysis for glucose using an amperometric enzyme electrode based on lipid-modified glucose oxidase as the detector," Biosens. Bioelectron. **9**, 411–414 (1994).
[26]C. Huang, Y. Chen, C. Wang, T. Chou, and G. Lee, "Integrated microfluidic systems for automatic glucose sensing and insulin injection," Sens. Actuators B **122**, 461–468 (2007).
[27]P. A. Serra, G. Rocchitta, G. Bazzu, A. Manca, G. M. Puggioni, J. P. Lowry, and R. D. O'Neill, "Design and construction of a low cost single-supply embedded telemetry system for amperometric biosensor applications," Sens. Actuators B **122**, 118–126 (2007).
[28]G. Calia, G. Rocchitta, R. Migheli, G. Puggioni, Y. Spissu, G. Bazzu, V. Mazzarello, J. Lowry, R. ONeill, M. Desole *et al*., "Biotelemetric monitoring of brain neurochemistry in conscious rats using microsensors and biosensors," Sensors **9**, 2511–2523 (2009).
[29]P. Serra, G. Puggioni, G. Bazzu, G. Calia, R. Migheli, and G. Rocchitta, *Design and Construction of a Distributed Sensor NET for Biotelemetric Monitoring of Brain Energetic Metabolism Using Microsensors and Biosensors* (InTech, 2010).
[30]O. Schuvailo, O. Soldatkin, A. Lefebvre, R. Cespuglio, and A. Soldatkin, "Highly selective microbiosensors for *in vivo* measurement of glucose, lactate and glutamate," Anal. Chim. Acta **573**, 110–116 (2006).
[31]See the supplementary material at http://dx.doi.org/10.1063/1.4705368 for supporting text and figures.
[32]Y. N. Xia and G. M. Whitesides, "Soft lithography," Angew. Chem., Int. Ed. **37**, 551–575 (1998).
[33]J. McDonald and G. Whitesides, "Poly (dimethylsiloxane) as a material for fabricating microfluidic devices," Acc. Chem. Res. **35**, 491–499 (2002).
[34]M. Unger, H. Chou, T. Thorsen, A. Scherer, and S. Quake, "Monolithic microfabricated valves and pumps by multilayer soft lithography," Science **288**, 113–116 (2000).
[35]H. Chou, M. Unger, and S. Quake, "A microfabricated rotary pump," Biomed. Microdevices **3**, 323–330 (2001).
[36]*Handbook of Chemistry and Physics*, edited by R. C. Weast, 53rd ed. (The Chemical Rubber Publishing, 1972).
[37]E. L. Cussler, *Diffusion Mass Transfer in Fluid Systems* (Cambridge University Press, 1984).
[38]S. Van Stroe-Biezen, F. Everaerts, L. Janssen, and R. Tacken, "Diffusion coefficients of oxygen, hydrogen peroxide and glucose in a hydrogel," Anal. Chim. Acta **273**, 553–560 (1993).
[39]P. Nien, P. Chen, C. Hsu, and K. Ho, "On-chip glucose biosensor based on enzyme entrapment with pre-reaction to lower interference in a flow injection system," Sens. Actuators B **157**, 64–71 (2011).
[40]M. Rahman, P. Kumar, D. Park, and Y. Shim, "Electrochemical sensors based on organic conjugated polymers," Sensors **8**, 118–141 (2008).
[41]P. Miller, S. Gittard, T. Edwards, D. Lopez, X. Xiao, D. Wheeler, N. Monteiro-Riviere, S. Brozik, R. Polsky, and R. Narayan, "Integrated carbon fiber electrodes within hollow polymer microneedles for transdermal electrochemical sensing," Biomicrofluidics **5**, 013415 (2011).
[42]J. Yan, V. Pedrosa, J. Enomoto, A. Simonian, and A. Revzin, "Electrochemical biosensors for on-chip detection of oxidative stress from immune cells," Biomicrofluidics **5**, 032008 (2011).